GEOMETRY DESIGN AND ANALYSIS FOR TROCHOIDAL-TYPE SPEED REDUCERS: WITH CONJUGATE ENVELOPES

Yii-Wen Hwang, Chiu-Fan Hsieh
Department of Mechanical Engineering, National Chung-Cheng University,
168 San-Hsing, Ming-Hsiung, Chia-Yi 621, Taiwan, R.O.C.
E-mail address: imeywh@ccu.edu.tw (**Y.W. Hwang**), naturaltom@gmail.com (**C.F. Hsieh**).

Received November 2005, Accepted April 2006
No. 05-CSME-59, E.I.C. Accession 2911

ABSTRACT

This paper illustrates the use of the envelope theorem for the geometric design of a cycloidal speed reducer. Specifically, it proposes two designs for a mathematical model with tooth differences: a pin wheel epitrochoid meshing – which is a cycloidal wheel (internal rotor) profile equidistant to an epitrochoid (or extended epicycloid) curve and a cycloidal wheel is generated by a pin wheel (external rotor) – and a pin wheel hypotrochoid meshing. These two contrasting structures differ in their equidistance to the epitrochoid (or extended epicycloid) curve and hypotrochoid (or extended hypocycloid) curve. Using the design result parameters, the analysis also compares contact forces and assesses curvature to determine whether the cycloidal wheel has a non-undercutting or continuous condition.

Keywords : cycloidal speed reducer; envelope; contact forces analysis; curvature; undercutting

CONCEPTION ET ANALYSE GÉOMETRIQUE POUR LE TYPE DE TROCHOÏDE RÉDUCTEURS DE VITESSE AVEC ENVELOPPES CONJUGUÉES

RESUME

Cette étude démontre l'utilisation du théorème d'enveloppe pour la conception géométrique d'un réducteur cycloïdal de vitesse. Plus particulièrement, il propose deux conceptions pour un modèle mathématique avec des différences de dent : une goupille engrenée épitrochoïde de roue – qui est un profil cycloïdal de roue (rotor interne) équidistant à une courbe épitrochoïde (ou épicycloïde prolongée) et une roue cycloïdale produite par une goupille roue (rotor externe) – et une goupille de roue engrenée hypotrochoïde. Ces deux structures contrastantes diffèrent dans leur équidistance à la courbe épitrochoïde (ou épicycloïde prolongée) et à la courbe hypotrochoïde (ou hypocycloïde prolongée). Utilisant les paramètres résultants, l'analyse compare également les forces de contact et évalue la courbure afin de déterminer si la roue cycloïdale est en non-dégagement ou en état continu.

Mots-clés : réducteur cycloïdal de vitesse ; enveloppe ; analyse des forces de contact ; courbure ; dégagement

1. INTRODUCTION

As shown in Fig. 1, cycloidal speed reducers, which belong to the category of planetary rotation machines, are composed of four main elements : (1) an input apparatus, (2) a cycloidal disc, (3) ring gear rollers (pins), and (4) an output apparatus. As the input shaft turns, the eccentric bearing goes into a rocking motion that exerts an outward radial force on the cycloidal disc. As the eccentric bearing turns to transmit torque and provide speed reduction, the cycloidal disc, confined inside the ring-gear housing with pins, begins a planetary motion. Because a cyclo drive and high-strength material are used in their high precision manufacture, cycloidal reducers offer the advantage of a high reduction ratio and high efficiency, a compact construction and a small volume and lower weight. Additionally, they are based on rolling mesh theory, which decreases the sliding friction and the oscillation phenomenon. Thus, the cycloidal speed reducer has a long life and is widely used in heavy industry such as crane transportation, boats, metallurgical mining and the oil chemical industry.

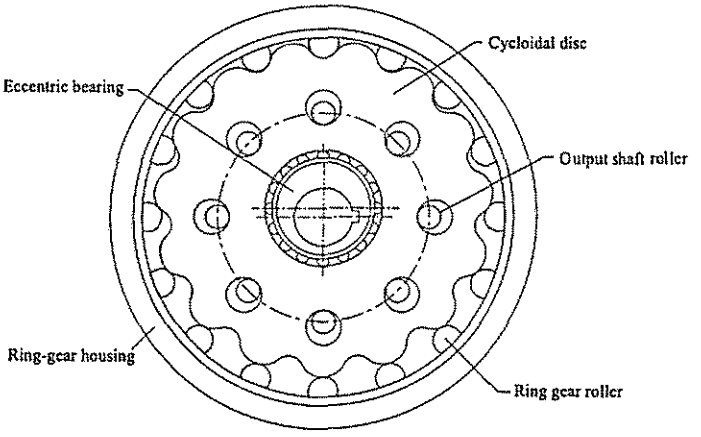

Fig. 1 Schematic of a cycloidal speed reducer

The relevant research on cycloidal drives includes Yang and Blanche's [1] investigation of the characteristics of the backlash and torque ripple and the relationships among machining tolerance, drive parameters (i.e. gear ratio, pitch diameter and normalized tooth heights) and drive performance indices (i.e. backlash and torque ripple). Tsay and Yu [2,3] proposed an analytical method for gerotors with outer rotor arc teeth and inner rotor trochoid teeth and compared the relations among variables in the traditional design method with those of their proposed method. They concluded that, as a gerotor cannot be adjusted to compensate for wear, the contact forces should be kept to a minimum and the lobe curvature decreased to reduce the wear rate. From this, Beard, Yannitell and Pennock [4] derived relationships showing the influence of the trochoid ratio, the pin size ratio and the radius of the generating pin on the curvature of the epitrochoidal gerotor. Litvin and Feng [5], who developed computer programs for generating the planar cycloidal gearings and rotors of screw Root's blowers, also presented an improved design that eliminated profile and surface singularities. Fong and Tsay [6] proposed using the dimensionless equation of non-undercutting to study the feasible design region without undercutting for the internal cycloidal gear with a small tooth difference. However, whereas the above studies focus on the pin wheel (outer rotor arc teeth) outside the cycloidal wheel (inner rotor trochoid teeth), more recent studies have demonstrated the feasibility of examining the inside of the cycloidal wheel. For example, Yan and Lai [7] and Lai [8] used the theory of conjugate surfaces and a CAD software package to produce a geometric design procedure for roller drives with cylindrical meshing elements. Using finite differences to obtain the cycloidal

profile curvature, they found that the pinion-tooth curvature must be larger or equal to it.

For the two design types presented here – pin wheel epitrochoid meshing and pin wheel hypotrochoid meshing – we derive a mathematical model with tooth difference using coordinate transformation and the envelope theorem for the cycloidal speed reducer profile. The following sections present the results of these two designs, followed by contact force comparisons and an analysis of curvature and the undercutting conditions.

2. GEOMETRIC DESIGN

The fundamentals of pin wheel epitrochoid meshing and pin wheel hypotrochoid meshing are illustrated in Figs. 2(a) and 2(b), respectively. An epitrochoid and a hypotrochoid is each defined as a path, which is traced by a point lying inside the rolling circle that rotates outside and inside, respectively, of a base circle circumference. If the epitrochoid and hypotrochoid paths are assumed to be the center of the rollers, the cycloidal wheel profile (the generated shape) can be produced by the inner and outer envelope methods.

There are, however, two other methods that can generate the cycloidal wheel. One alternative for producing pin wheel epitrochoid meshing is illustrated in Fig. 3(a), in which circles 1 and 2 are in internal tangency and have separate radii ρ_1 and ρ_2, respectively. Point I is the instantaneous center of rotation. When circle 1 rotates counter-clockwise around the circumference of circle 2 in a pure rolling motion, the eccentric throw r is the distance between point p and the center of circle 1, and point p will generate an extended epicycloid path. Similarly, as shown in Fig. 3(b), in the pin wheel hypotrochoid meshing design, point q will generate an extended hypocycloid path. Therefore, the extended epicycloid and extended hypocycloid paths could be the center of the rollers, meaning that the cycloidal wheel profile can be generated by the inner and outer envelope methods. In other words, the cycloidal wheel profile will be produced using the inward equidistance to the extended epicycloid and the outward equidistance to the extended hypocycloid. Here, the rollers are the same as the pins.

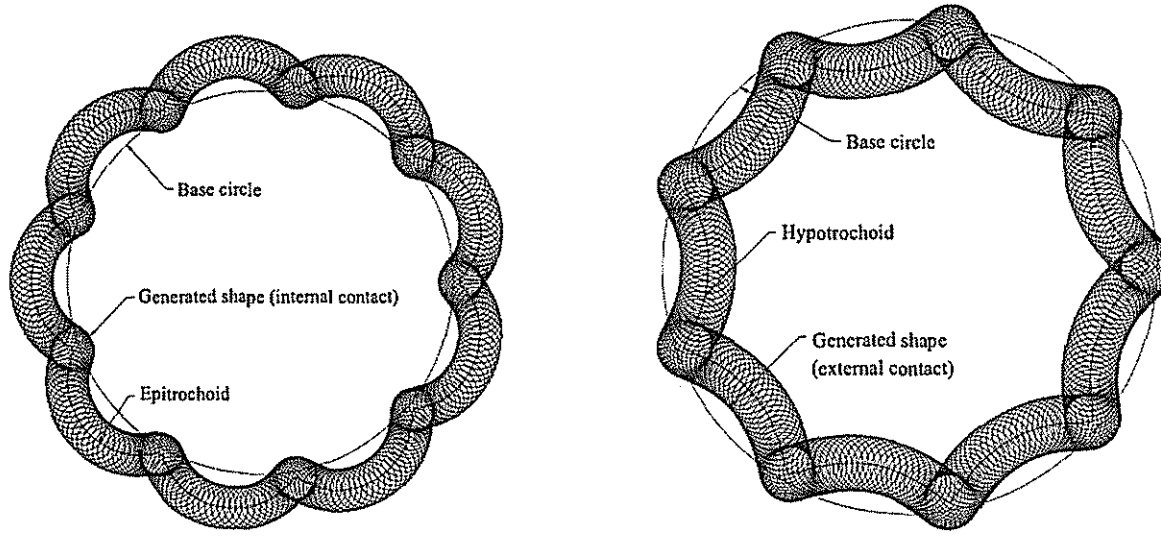

(a) Pin wheel epitrochoid meshing (b) Pin wheel hypotrochoid meshing

Fig. 2 Basic idea of cycloidal speed reducer

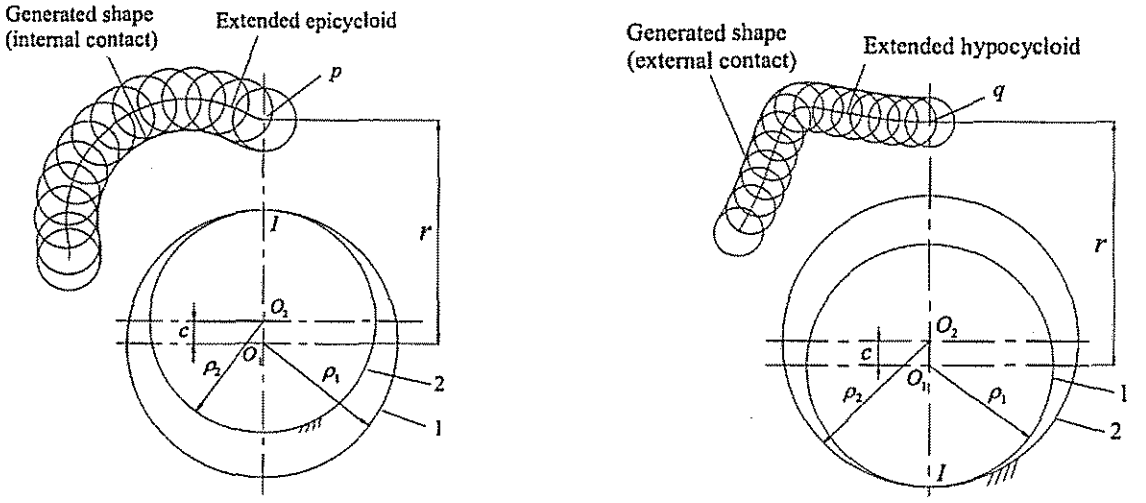

(a) The extended epicycloidal curve (b) The extended hypocycloidal curve

Fig. 3 Generation of trochoidal curve

2.1 Mathematical Model of Pin Wheel Epitrochoid Meshing

The mathematical model of pin wheel epitrochoid meshing is derived based on the above ideas. As shown in Fig. 4, the coordinate systems S_1, S_2 and S_f are rigidly attached to the pin wheel, the cycloidal wheel and the frame, respectively.

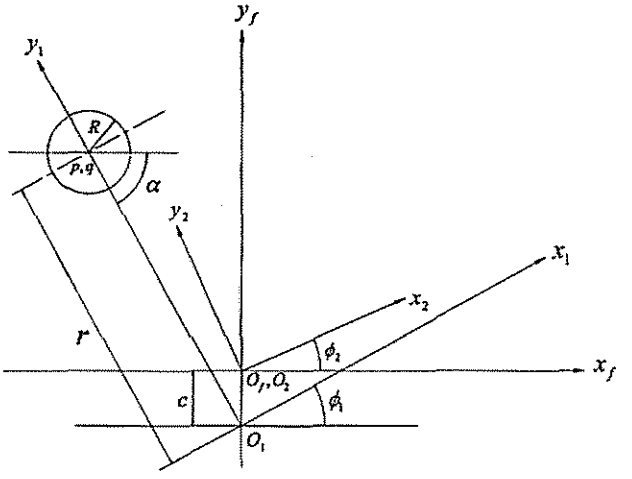

Fig. 4 Applied coordinate systems

The ratio of the rotation angle in the pin wheel and the cycloidal wheel is inversely proportional to the ratio of the tooth number. Therefore, the relationship between the rotation angles ϕ_2 and ϕ_1 is represented by the following:

$$\phi_2 = \frac{N}{N-m}\phi_1 \tag{1}$$

where N is the tooth number of the pin wheel and m is the tooth number difference between the pin wheel and the cycloidal wheel. Thus, the tooth number of the cycloidal wheel is $N-m$.

We first consider the case in which the extended epicycloidal curve is generated in coordinate system s_2 by point p, which is rigidly connected to the coordinate system s_1. Point p is represented in s_1 as follows:

$$\mathbf{r}_1^{(p)} = \begin{bmatrix} 0 & r & 1 \end{bmatrix}^T \tag{2}$$

The equation of the extended epicycloidal curve can be determined by the following coordinate transformation:

$$\mathbf{r}_2^{(p)} = \mathbf{M}_{21}\mathbf{r}_1^{(p)} = \mathbf{M}_{2f}\mathbf{M}_{f1}\mathbf{r}_1^{(p)} \tag{3}$$

where

$$\mathbf{M}_{2f} = \begin{bmatrix} \cos\left(\frac{N}{N-m}\phi_1\right) & \sin\left(\frac{N}{N-m}\phi_1\right) & 0 \\ -\sin\left(\frac{N}{N-m}\phi_1\right) & \cos\left(\frac{N}{N-m}\phi_1\right) & 0 \\ 0 & 0 & 1 \end{bmatrix}, \quad \mathbf{M}_{f1} = \begin{bmatrix} \cos\phi_1 & -\sin\phi_1 & 0 \\ \sin\phi_1 & \cos\phi_1 & -c \\ 0 & 0 & 1 \end{bmatrix}$$

The mathematical equation of the extended epicycloidal curve can be yielded from Eq. (3) as follows:

$$\mathbf{r}_2^{(p)} = \begin{bmatrix} r_{x2}^{(p)} \\ r_{y2}^{(p)} \\ 1 \end{bmatrix} = \begin{bmatrix} r\sin\left(\frac{m}{N-m}\phi_1\right) - c\sin\left(\frac{N}{N-m}\phi_1\right) \\ r\cos\left(\frac{m}{N-m}\phi_1\right) - c\cos\left(\frac{N}{N-m}\phi_1\right) \\ 1 \end{bmatrix} \tag{4}$$

The unit normal vector of Eq. (4) can then be derived by the following:

$$\mathbf{n}_2^{(p)} = \frac{\frac{\partial \mathbf{r}_2^{(p)}}{\partial \phi_1} \times \mathbf{k}}{\left|\frac{\partial \mathbf{r}_2^{(p)}}{\partial \phi_1}\right|} = \begin{bmatrix} n_{x2}^{(p)} \\ n_{y2}^{(p)} \\ 0 \end{bmatrix} \tag{5}$$

where

$$\frac{\partial \mathbf{r}_2^{(p)}}{\partial \phi_1} = \begin{bmatrix} T_{x2}^{(p)} \\ T_{y2}^{(p)} \\ 0 \end{bmatrix} = \begin{bmatrix} \frac{1}{N-m}\left[mr\cos\left(\frac{m}{N-m}\phi_1\right) - cN\cos\left(\frac{N}{N-m}\phi_1\right)\right] \\ \frac{1}{N-m}\left[-mr\sin\left(\frac{m}{N-m}\phi_1\right) + cN\sin\left(\frac{N}{N-m}\phi_1\right)\right] \\ 1 \end{bmatrix}, \left|\frac{\partial \mathbf{r}_2^{(p)}}{\partial \phi_1}\right| = \left[\left(T_{x2}^{(p)}\right)^2 + \left(T_{y2}^{(p)}\right)^2\right]^{\frac{1}{2}}$$

Because it may have either a positive or negative value, the equation of the cycloidal wheel profile can be represented in S_2 as follows:

$$\mathbf{r}_2 = \begin{bmatrix} r_{x2}^{(p)} + n_{x2}^{(p)} R \\ r_{y2}^{(p)} + n_{x2}^{(p)} R \\ 1 \end{bmatrix} \tag{6}$$

We can then substitute Eqs. (4) and (5) into Eq. (6) to yield the cycloidal wheel profile. If Eq. (6) is assumed to be the equation of the envelope, we can analyze the curvature of the cycloidal wheel by first considering the curvature of the extended epicycloidal curve and then deriving the following equation of curvature:

$$\kappa_2^{(p)}(\phi_1) = \frac{\mathbf{g}_{\phi\phi} \cdot \mathbf{n}_2^{(p)}}{\left|\mathbf{g}_{\phi_1}\right|^2} \tag{7}$$

where

$$\mathbf{g}_{\phi_1} = \frac{\partial \mathbf{r}_2^{(p)}}{\partial \phi_1}, \quad \mathbf{g}_{\phi\phi} = \frac{\partial^2 \mathbf{r}_2^{(p)}}{\partial \phi_1^{\,2}}$$

Operating Eq. (7) yields:

$$\kappa_2^{(p)} = \frac{c^2N^3 + m^3r^2 - cmNr(N+m)\cos\phi_1}{\left[(cN)^2 + (mr)^2 - 2cmNr\cos\phi_1\right]^{3/2}} \tag{8}$$

Even though Eq. (8) may imply a positive or a negative value, it does delineate the differences between the curvature of the cycloidal wheel profile and the extended epicycloidal curve. Therefore, the curvature of the cycloidal wheel profile is determined as follows:

$$\kappa = \frac{\kappa_2^{(p)}}{1 - R\kappa_2^{(p)}} \tag{9}$$

2.2 Mathematical Model of Pin Wheel Hypotrochoid Meshing

If we design the pin wheel to be the inner rotor, the applied coordinate systems are as shown in Fig. 4, with only the following difference between rotation angles ϕ_2 and ϕ_1:

$$\phi_2 = \frac{N}{N+m}\phi_1 \tag{10}$$

where N is also the tooth number of the pin wheel. Similarly, the extended hypocycloidal curve is generated in coordinate system s_2 by point q, which is rigidly connected to the coordinate system s_1. Point q is represented in s_1 as Eq. (2), and operating the coordinate transformation as Eq. (3) yields the following:

$$\mathbf{r}_2^{(q)} = \begin{bmatrix} -r\sin\left(\frac{m}{N+m}\phi_1\right) - c\sin\left(\frac{N}{N+m}\phi_1\right) \\ r\cos\left(\frac{m}{N+m}\phi_1\right) - c\cos\left(\frac{N}{N+m}\phi_1\right) \\ 1 \end{bmatrix} \tag{11}$$

where

$$\mathbf{M}_{2f} = \begin{bmatrix} \cos\left(\frac{N}{N+m}\phi_1\right) & \sin\left(\frac{N}{N+m}\phi_1\right) & 0 \\ -\sin\left(\frac{N}{N+m}\phi_1\right) & \cos\left(\frac{N}{N+m}\phi_1\right) & 0 \\ 0 & 0 & 1 \end{bmatrix}, \quad \mathbf{M}_{f1} = \begin{bmatrix} \cos\phi_1 & -\sin\phi_1 & 0 \\ \sin\phi_1 & \cos\phi_1 & -c \\ 0 & 0 & 1 \end{bmatrix}$$

Similarly, the unit normal vector may be yielded as Eq. (5). Taking Eq. (6) into consideration, we then substitute Eq. (11) into Eq. (5) to yield the cycloidal wheel profile, where

$$\frac{\partial \mathbf{r}_2^{(q)}}{\partial \phi_1} = \begin{bmatrix} \frac{1}{N+m}\left[-mr\cos\left(\frac{m}{N+m}\phi_1\right) - cN\cos\left(\frac{N}{N+m}\phi_1\right)\right] \\ \frac{1}{N+m}\left[-mr\sin\left(\frac{m}{N+m}\phi_1\right) + cN\sin\left(\frac{N}{N+m}\phi_1\right)\right] \\ 0 \end{bmatrix}, \quad \left|\frac{\partial \mathbf{r}_2^{(q)}}{\partial \phi_1}\right| = \left[\left(T_{x2}^{(q)}\right)^2 + \left(T_{y2}^{(q)}\right)^2\right]^{\frac{1}{2}}$$

The equation of curvature can be derived as in Eq. (7), which yields

$$\kappa_2^{(q)} = \frac{c^2N^3 - m^3r^2 + cmNr(N-m)\cos\phi_1}{\left[(cN)^2 + (mr)^2 + 2cmrN\cos\phi_1\right]^{3/2}} \tag{12}$$

Even though Eq. (12) may imply a positive or a negative value, it does designate the difference between the curvatures of the cycloidal wheel profile and the extended hypocycloidal curve. Thus, the curvature of the cycloidal wheel profile is also determined as

$$\kappa = \frac{\kappa_2^{(q)}}{1 - R\kappa_2^{(q)}} \tag{13}$$

The design results are shown in Figs. 5 and 6. Because Fig. 5(a)–(d) corresponds to Fig. 6(a)–(d), Fig. 5(a) and Fig. 6(a) have the same design parameter values. Therefore, we can obtain the design differences between these two models for the cycloidal speed reducer.

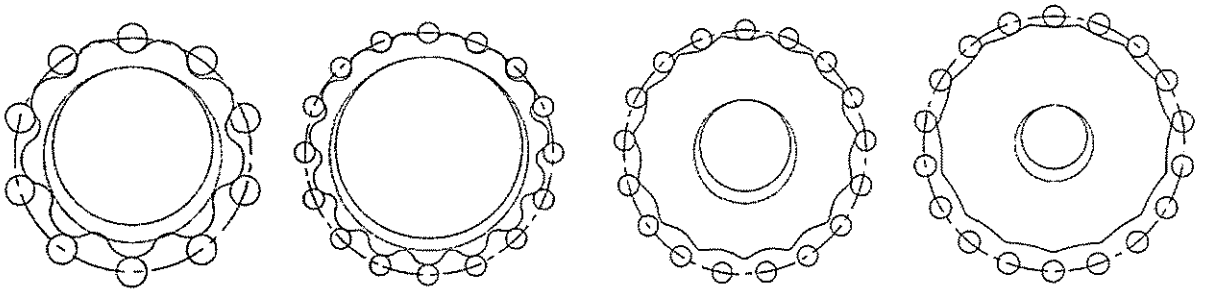

(a) c=3,m=1,N=10,r=40,R=5 (b) c=3,m=1,N=16,r=60,R=5 (c) c=3,m=2,N=17,r=60,R=5 (d) c=3,m=3,N=18,r=60,R=5

Fig. 5 Design results of pin wheel epitrochoid meshing

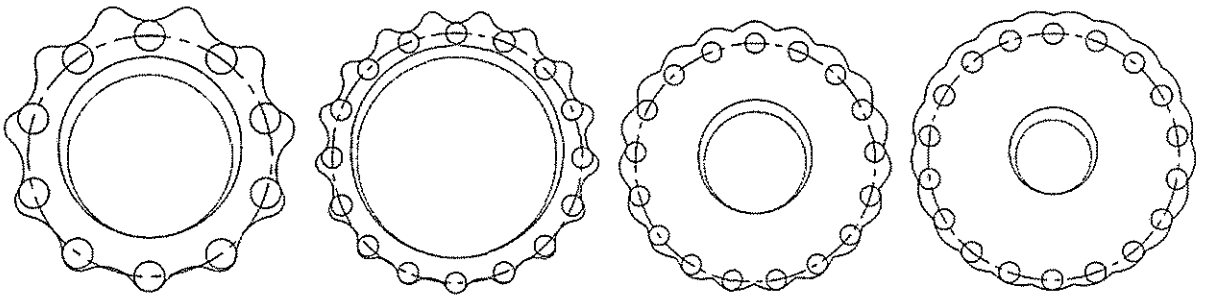

(a) c=3,m=1,N=10,r=40,R=5 (b) c=3,m=1,N=16,r=60,R=5 (c) c=3,m=2,N=17,r=60,R=5 (d) c=3,m=3,N=18,r=60,R=5

Fig. 6 Design results of pin wheel hypotrochoid meshing

3. THE CONTACT FORCES OF THE PIN WHEEL

The contact positions between the pin wheel and the cycloidal wheel are illustrated in Figs. 7(a) and 7(b). We know from the contact force analysis that the contact forces in all pins are in tangency with all cycloidal curves (disregarding misalignment and manufacturing errors). However, only half can be under load and less than half due to misalignment. The directions of the contact forces all run from the contact points to pitch point *I* and can pass through the centre of the rollers (pins).

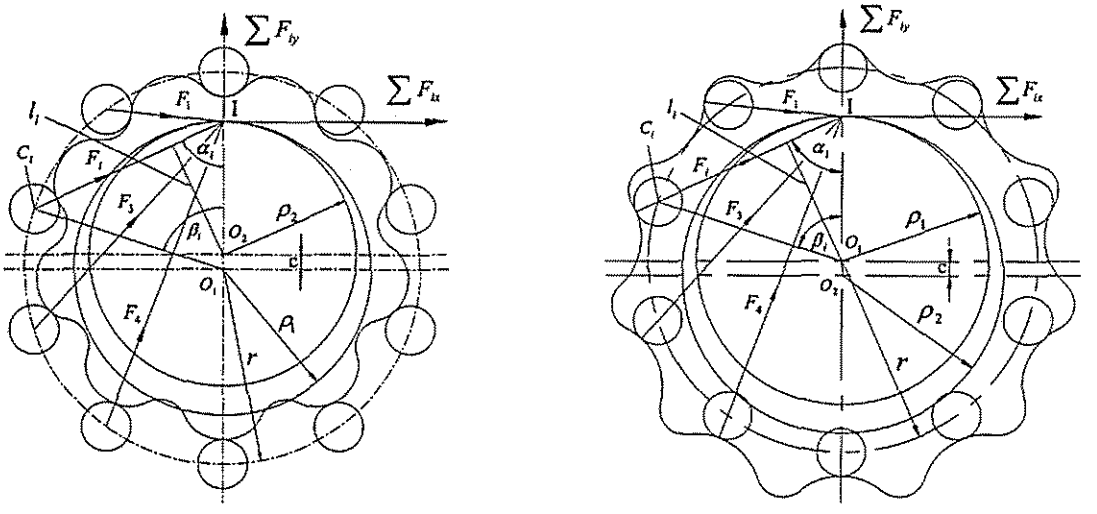

(a) The outer pin wheel (b) The inner pin wheel

Fig. 7 Contact forces of the cycloidal speed reducer

When the axes of the pin wheel and cycloidal wheel are fixed, if the output shaft exerts a counter-clockwise torque T on the cycloidal wheel, it actually only exerts a half torque (T_x=T/2) (see Fig. 7(a)) because only half the pins are under load [10]. In the same way, it will also only exert a half torque (T_x=T/2) on the pin wheel (see Fig. 7(b)). In these cases, ρ_1 and ρ_2 are the individual pitch radii of the pin wheel and the cycloidal wheel, respectively. Assuming z_1 to be the tooth number of the pin wheel and z_2 that of the cycloidal wheel, the tooth number difference and the eccentric distance are separately represented as $m=|z_1-z_2|$ and $c=|\rho_1-\rho_2|$, respectively.

The formulas for contact forces [10] are represented as follows:

$$F_{\max}=\frac{4\times10^3 T_x}{\lambda z r} \tag{14}$$

$$F_i=F_{\max}\sin\alpha_i \tag{15}$$

$$T_i=F_i l_i \tag{16}$$

$$T_x=\sum T_i \tag{17}$$

Here, z is the tooth number of the inner rotor and the shortened cycloid ratio λ is defined in the following manner:

$$\lambda = \frac{\rho_1}{r} \tag{18}$$

The pitch radius of the pin wheel is then derived as

$$\rho_1 = \frac{cN}{m} \tag{19}$$

In the pin wheel epitrochoid meshing design (see Fig. 7(a)), in which the cycloidal wheel is the inner rotor, z will equal z_2. Letting $\overline{C_iI} = d$, we determine the following equations from the relation of the triangular geometry:

$$d = \sqrt{\rho_1^2 + r^2 - 2\rho_1 r\cos\beta_i} \tag{20}$$

$$\beta_i = \frac{360}{z_1} i \tag{21}$$

$$\alpha_i = \sin^{-1}\left(\frac{r\sin\beta_i}{d}\right) \tag{22}$$

$$\rho_2 = \rho_1 - c \tag{23}$$

$$l_i = \rho_2 \sin\alpha_i \tag{24}$$

where $i = 1 \sim \frac{z_1}{2}$.

Likewise, in the pin wheel hypotrochoid meshing design (see Fig. 7(b)), in which the pin wheel is the inner rotor, z equals z_1. Thus, letting $\overline{C_iI} = e$, we determine the following equations from the relation of the triangular geometry:

$$e = \sqrt{\rho_1^2 + r^2 - 2\rho_1 r\cos\beta_i} \tag{25}$$

$$\alpha_i = \sin^{-1}\left(\frac{r\sin\beta_i}{e}\right) \tag{26}$$

$$l_i = \rho_1 \sin\alpha_i \tag{27}$$

where β_i is the same as in Eq. (21) and $i = 1 \sim z_1/2$.

To obtain the contact force analysis for the pin wheels in the two types of speed reducers, we must first calculate these parameters (β_i, α_i and l_i) and then substitute them into Eqs.

(14)–(27).

Next, to clearly compare the contact forces of the pin wheel epitrochoid meshing with those of the pin wheel hypotrochoid meshing, we consider the parameter values given in Table 1. The analysis of contact forces is shown here by the differences for one tooth number and two tooth numbers under the same output conditions of 981 N-m and 1800 RPM-12.4 HP.

The contact force results for the one tooth number and two tooth numbers differences are shown in Fig. 8. Given the same tooth number for pin wheel z_1, because the contact amount of the pins in $m=1$ is larger than that in $m=2$, the forces in $m=1$ are smaller than those in $m=2$ for every pin number. Additionally, for either $m=1$ or $m=2$, the inner pin wheel design produces a smaller contact force than the outer pin wheel design, meaning an improvement in the speed reducer's transmission efficiency and an increase in its usage life.

Table 1 Designed parameters

Case 1 (outer pin)	$m=1,\ z_1=36,\ z_2=35,\ R=5$ $r=140,\ c=3,\ \lambda=0.771$	Case 2 (inner pin)	$m=1,\ z_1=36,\ z_2=37,\ R=5$ $r=140,\ c=3,\ \lambda=0.771$
Case 3 (outer pin)	$m=2,\ z_1=36,\ z_2=34, R=5$ $r=140,\ c=3,\ \lambda=0.386$	Case 4 (inner pin)	$m=2,\ z_1=36,\ z_2=38, R=5$ $r=140,\ c=3,\ \lambda=0.386$

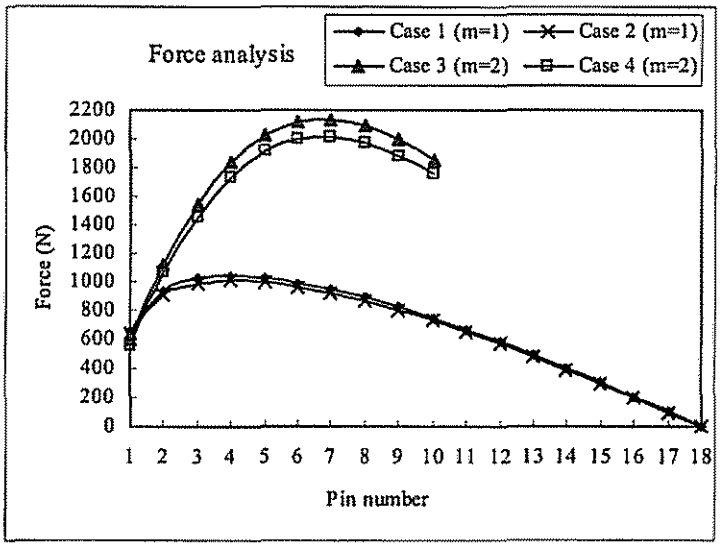

Fig. 8 Contact forces

It is known that decreasing the curvature of the cycloidal wheel profile can reduce the wear rate. If the curvature difference between pin wheel and cycloidal wheel is larger, then it can also reduce the wear rate. The curvature difference can then be represented as follows:

$$\kappa_d = \frac{1}{R} - \kappa \tag{28}$$

The wear rate can be further reduced by increasing the curvature difference to lower the Hertz stress. Because of the similarity of each lobe, we just analyze one of them. Figure 9 show the curvature difference analyses for the one tooth number and two tooth numbers differences.

Whether for $m=1$ or $m=2$, the inner pin wheel design attains a larger curvature difference than the outer pin wheel design in the design angle range, assigning even greater merit to the pin wheel hypotrochoid meshing design.

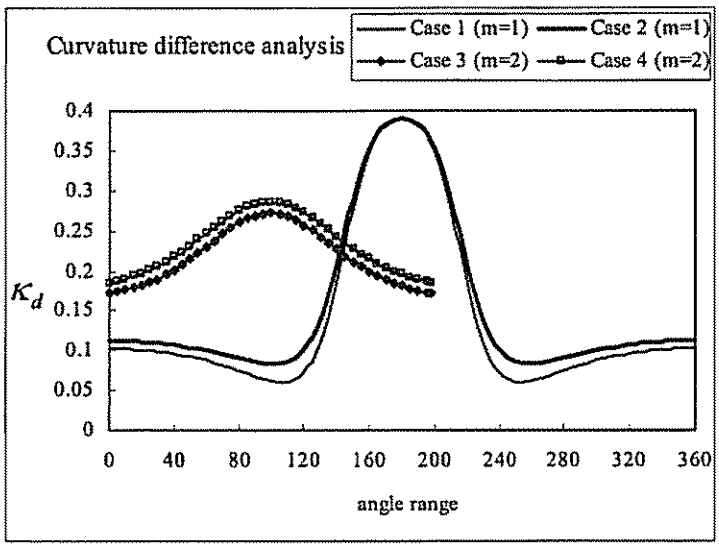

Fig. 9 Curvature difference

4. CURVATURE AND THE CONDITIONS OF THE UNDERCUTTING

Curvature analysis can reveal whether the curvature of the profile is quadratic continuous. If so, then the profile is quadratic continuous with no undercutting. Additionally, the curvature analysis can indicate not only the shape of the profile (a concave or convex curve) but the existence of an inflection point. Moreover, the undercutting conditions may be derived from the equation of curvature given in this paper.

4.1 Inflection Point

The possible conditions for the inflection point on the curve are that the curvature is equal to zero or the radius of curvature is infinitely great. Thus, for the extended hypocycloidal curve, Eq. (12) can be represented as

$$\kappa_2^{(q)} = \frac{c^2N^3 - m^3r^2 + cmNr(N-m)\cos\phi_1}{\left[(cN)^2 + (mr)^2 + 2cmrN\cos\phi_1\right]^{3/2}} = 0 \tag{29}$$

However, to obtain the condition of the inflection point, the numerator of Eq. (29) must be zero. Operating the equation thus yields

$$\phi_1 = \cos^{-1}\frac{m^3r^2 - c^2N^3}{cmNr(N-m)} \tag{30}$$

where the existence condition of the inflection point is

$$\left|\frac{m^3r^2 - c^2N^3}{cmNr(N-m)}\right| \leq 1 \tag{31}$$

Likewise, the condition of the inflection point for the extended epicycloidal curve is derived as

$$\phi_1 = \cos^{-1}\frac{m^3r^2 + c^2N^3}{cmNr(N+m)} \tag{32}$$

and the existence condition of its inflection point is

$$\left|\frac{m^3r^2 + c^2N^3}{cmNr(N+m)}\right| \leq 1 \tag{33}$$

Therefore, analyzing one lobe indicates that the inflection points may exit two angles ϕ_1 and $2\pi - \phi_1$.

4.2 Extreme Value of The Radius of Curvature

The radius of curvature on the extended hypocycloidal curve can be determined as follows:

$$\rho_2^{(q)} = \frac{1}{\kappa_2^{(q)}} \tag{34}$$

If the curve has an extreme value on the radius of curvature, it must satisfy the following:

$$\frac{\partial \rho_2^{(q)}}{\partial \phi_1} = 0 \tag{35}$$

Operating Eq. (35) yields

$$\frac{\Delta_1\Delta_2\Delta_3}{\Delta_4} = 0 \tag{36}$$

where

$$\Delta_1 = -cmNr\sin\phi_1 \tag{37}$$

$$\Delta_2 = \sqrt{(cN)^2 + (mr)^2 + 2cmNr\cos\phi_1} \tag{38}$$

$$\Delta_3 = (cN)^2(m+2N) - (mr)^2(2m+N) + cmNr(N-m)\cos\phi_1 \tag{39}$$

$$\Delta_4 = \left[c^2N^3 - m^3r^2 + cmNr(N-m)\cos\phi_1\right]^2 \tag{40}$$

However, to obtain the conditions of extreme value on the radius of curvature, the numerator of Eq. (36) must be zero, which can be achieved by any of the following three situations:

(1) $\Delta_1 = 0$

Eq. (37) yields the following angles:

$$\phi_1 = 0, \pi, 2\pi \tag{41}$$

(2) $\Delta_2 = 0$

Eq. (38) produces the following:

$$\cos\phi_1 = \frac{-(cN)^2 - (mr)^2}{2cmNr} = -\left(\frac{\mu^2+1}{2\mu}\right) < 0 \tag{42}$$

where $\mu = \dfrac{r}{\rho_1}$. Thus, from Eq. (42), we can write the following condition of existence:

$$\left|\cos\phi_1\right| = \left|-\left(\frac{\mu^2+1}{2\mu}\right)\right| \le 1 \tag{43}$$

However, the equation above is not existent when $0 < \mu < 1$ or $\mu > 1$ which caused $\left|\cos\phi_1\right| > 1$, so it is not easy to obtain the angle of the extreme value on the radius of curvature from Eq. (43). It exists only when $\mu = 1$ which makes $\left|\cos\phi_1\right| = 1$, and its angle of the extreme value on the radius of curvature is at $\phi_1 = \pi$ which leads to zero for the radius of curvature from Eqs. (12) and (34). Then that is a singular point. Therefore, the design $\mu = 1$ is not proposed.

(3) $\Delta_3 = 0$

The following equations can be derived from Eq. (39):

$$\begin{aligned} \cos\phi_1 &= \frac{-cN(m+2N)}{mr(N-m)} + \frac{mr(2m+N)}{cN(N-m)} \\ \phi_1 &= \cos^{-1}\left(\frac{-cN(m+2N)}{mr(N-m)} + \frac{mr(2m+N)}{cN(N-m)}\right) \end{aligned} \tag{44}$$

Substituting Eqs. (41) and (44) into Eq. (34), we find the minimum radius of curvature $\rho_2^{(q)}{}_{\min}$ that can be the extreme value on the pin radius in the pin wheel design. This value can be written as

$$R < \rho_2^{(q)}{}_{\min} \tag{45}$$

By the same token, the results of the extended epicycloidal curve are mostly the same as in Eq. (41), the difference being

$$\phi_1 = \cos^{-1}\left(\frac{cN(2N-m)}{mr(N+m)} + \frac{mr(2m-N)}{cN(N+m)}\right) \tag{46}$$

As above, we can then find the minimum radius of curvature $\rho_2^{(p)}{}_{\min}$ from Eqs. (41) and (46) to produce the following extreme value on the radius of the pin, R:

$$R < \rho_2^{(p)}{}_{\min} \tag{47}$$

Equations (45) and (47) can be the conditions for the design constraints without undercutting.

Based on these constraints, we also consider the parameter values given in Table 1. The results for the radius of curvature in the design range of a lobe are shown in Fig. 10 for trochoidal curves. When $\rho_2^{(p)}$ or $\rho_2^{(q)}$ are negative values, the curve is concave. Thus, the real profile of the cycloidal wheel is a concave curve and no undercutting occurs on the profile. Therefore, only when the values are positive do we discuss the undercutting condition. Given that $\rho_2^{(p)}{}_{\min} < \rho_2^{(q)}{}_{\min}$ ($m=1$ or $m=2$), the pin size could be designed to be larger, thereby increasing the strength of pin wheel hypotrochoid meshing.

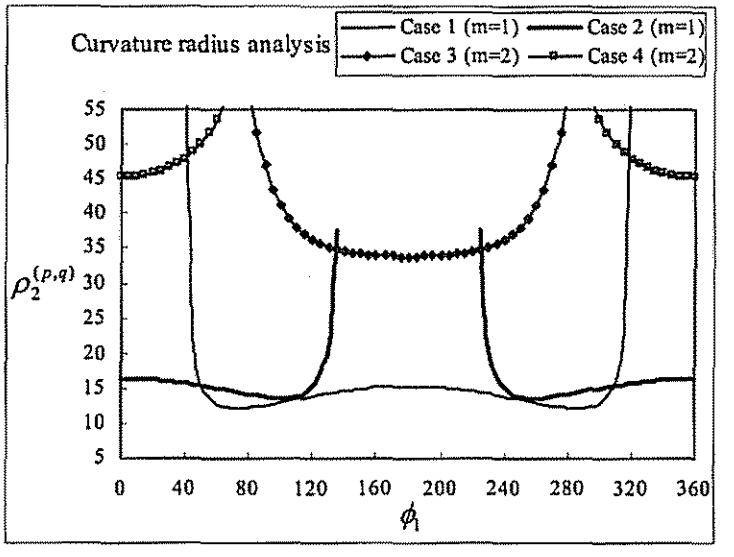

Fig. 10 Radius of curvature of trochoidal curve

The curvature of a cycloidal lobe under the four cases is shown in Fig. 11. Each case has two inflection points in each lobe. Moreover, all cases are continuous on the curvature; i.e. the pin sizes ($R=5$) are all smaller than their minimum radius of curvature. Additionally, the fact that the coefficients $\mu=1.296$ (for cases 1 and 2) and $\mu=2.593$ (for cases 3 and 4) are both larger than 1 [5] provides evidence that no undercutting exists in these cases. The calculated results are shown in Table 2.

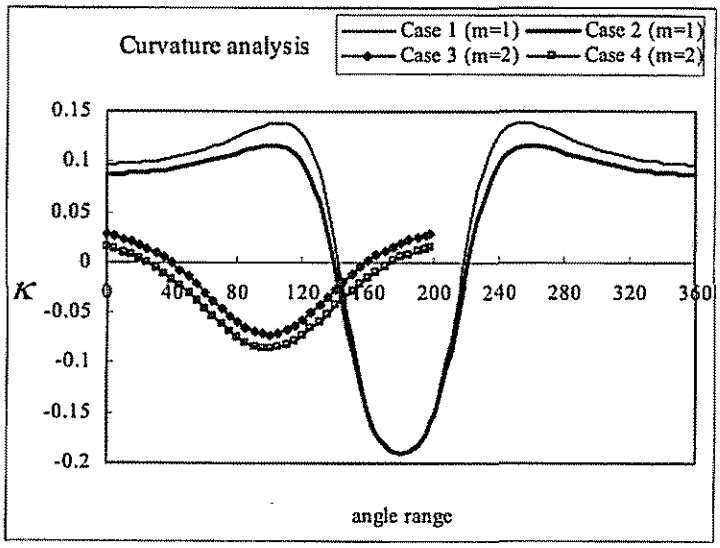

Fig. 11 Curvature of cycloidal wheel

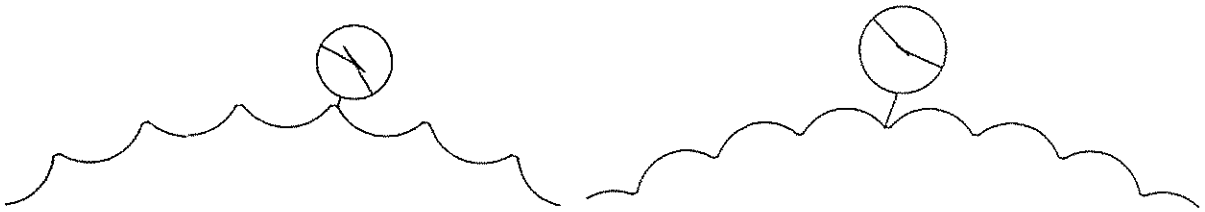

(a) Case 1 (b) Case 2

Fig. 12 Undercutting examples

Table 2 Calculated results

	Inflection point angle	Minimum curvature angle	Minimum curvature radius		Inflection point angle	Minimum curvature angle	Minimum curvature radius
Case 1 (outer pin)	38.223° 321.778°	73.185° 286.815°	12.168	Case 2 (inner pin)	139.151° 220.849°	101.629° 258.371°	13.598
Case 3 (outer pin)	59.873° 300.128°	180°	33.845	Case 4 (inner pin)	104.827° 255.173°	0° 360°	45.237

When the pin size (R) is larger than the minimum radius of curvature – e.g. for one tooth difference – and the values of (R) are as 13 and 14 in case 1 and case 2, respectively, we can

prove the undercutting phenomenon as illustrated in Fig. 12.

5. CONCLUSION

In this paper, we present a mathematical model of trochoidal curves in parametric form and use the envelope method to produce a real cycloidal wheel profile. We also derive and discuss the inflection points and curvature of trochoidal curves and their equidistance. The design constraints we derive from the equation of curvature for the trochoidal curves. Based on our contact force and curvature analysis, we conclude that, given the same parameter conditions, the pin wheel hypotrochoid meshing design is superior to the pin wheel epitrochoid meshing design. Specifically, the greater strengths of the pin wheel hypotrochoid meshing design include lower contact force, lower curvature on the cycloidal wheel profile and a larger difference in curvature between the pin wheel and the cycloidal wheel. The results clearly show that this proposed design model can help reduce the speed reducers' wear rate, thereby improving its motion efficiency and increasing its usage life.

NOMENCLATURE

c	center distance between the pin wheel and the cycloidal wheel
m	the tooth numbers difference between the pin wheel and the cycloidal wheel
N	the tooth number of the pin wheel
R	pin radius
r	center distance between the pin and the pin wheel
S_i	coordinate system i where $i = 1,2,f$
O_i	origin of the coordinate system S_i, $i = 1,2,f$
ϕ_i	rotation angle, $i = 1,2$
$\mathbf{M}_{ij}$	coordinate transformation matrix from system j to system i
$\mathbf{r}_1^{(j)}$	point j represented in S_1, $j = p,q$
$\mathbf{r}_2^{(j)}$	position vector of trochoidal curve represented in S_2, $j = p,q$
$\kappa_2^{(j)}$	curvature of trochoidal curve, $j = p,q$
κ	curvature of the cycloidal wheel
κ_d	curvature difference between the pin wheel and the cycloidal wheel
ρ_1	pitch radius of the pin wheel
ρ_2	pitch radius of the cycloidal wheel
$\rho_2^{(j)}$	radius of curvature of trochoidal curve, $j = p,q$
$\rho_{2\,\min}^{(j)}$	minimum radius of curvature of trochoidal curve, $j = p,q$

REFERENCES

1. Yang, D. C. H. and Blanche, J. G., Design And Application Guidelines For Cycloid Drives With Machining Tolerances, Mechanism and Machine Theory, Vol.25, 1990, pp.487-501.
2. Tsay, C. B. and Yu, C. Y., Mathematical Model for the Profile of Gerotor Pumps, Journal of the Chinese Society of Mechanical Engineers, Vol.10, 1989, pp.41-47.
3. Tsay, C. B. and Yu, C. Y., The Mathematical Model of Gerotor Pump Applicable to Its Characteristic Study, Journal of the Chinese Society of Mechanical Engineers, Vol.11, 1990, pp.385-391.
4. Beard, J. E., Yannitell, D. W. and Pennock, G. R., The Effect of the Generating Pin Size And Placement On the Curvature And Displacement of Epitrochoidal Gerotors, Mechanism and Machine Theory, Vol.27, 1992, pp.373-389.
5. Litvin, F. L. and Feng, P. H., Computerized Design And Generation of Cycloidal Gearings, Mechanism and Machine Theory, Vol.31, 1996, pp.891-911.
6. Fong, Z. H. and Tsay, C. W., Study on the Undercutting of Internal Cycloidal Gear with Small Tooth Difference, Journal of the Chinese Society of Mechanical Engineers, Vol.21, 2000, pp.359-367.
7. Yan, H. S. and Lai, T. S., Geometry design of an elementary planetary gear train with cylindrical tooth-profiles, Mechanism and Machine Theory, Vol.37, 2002, pp.757-767.
8. Lai, T. S., Geometric design of roller drives with cylindrical meshing elements, Mechanism and Machine Theory, Vol.40, 2005, pp.55-67.
9. Litvin, F. L., *Theory of Gearing*, NASA Reference Publication 1212, Washington D. C., 1989.
10. Editorial committee of the gear handbook, *Gear handbook (3)*, China Machine Press., 1994.